Insights into the composition of ancient Egyptian red and black inks on papyri achieved by synchrotron-based microanalyses

Thomas Christiansen[a,1,2], Marine Cotte[b,c,1,2], Wout de Nolf[b], Elouan Mouro[b], Juan Reyes-Herrera[b], Steven de Meyer[d,e], Frederik Vanmeert[d,e], Nati Salvadó[f], Victor Gonzalez[g], Poul Erik Lindelof[h,i], Kell Mortensen[h], Kim Ryholt[a], Koen Janssens[d,e], and Sine Larsen[j]

[a]Egyptology Section, Department of Cross-Cultural and Regional Studies, University of Copenhagen, 2300 Copenhagen S, Denmark; [b]The European Synchrotron Radiation Facility, 38043 Grenoble Cedex 9, France; [c]Laboratoire d'Archéologie Moléculaire et Structurale, University of Sorbonne, Pierre and Marie Curie University Paris 06, CNRS, UMR 8220, 75005 Paris, France; [d]Antwerp X-Ray Analysis, Electrochemistry & Speciation Research Group, Department of Physics, University of Antwerp, 2020 Antwerp, Belgium; [e]NanoLab Centre of Excellence, University of Antwerp, 2020 Antwerp, Belgium; [f]Departament d'Enginyeria Química, Escola Politècnica Superior d'Enginyeria de Vilanova i la Geltrú, Polytechnic University of Catalonia, 08800 Vilanova i la Geltrú, Barcelona, Spain; [g]Science Department, Rijksmuseum, 1071 ZC, Amsterdam, The Netherlands; [h]Niels Bohr Institute, University of Copenhagen, 2100 Copenhagen Ø, Denmark; [i]Ancient Cultures of Denmark and the Mediterranean, National Museum of Denmark, 1471 Copenhagen K, Denmark; and [j]Department of Chemistry, University of Copenhagen, 2100 Copenhagen Ø, Denmark

Edited by Katherine Faber, California Institute of Technology, Pasadena, and accepted by Editorial Board Member Tobin J. Marks September 21, 2020 (received for review March 10, 2020)

A hitherto unknown composition is highlighted in the red and black inks preserved on ancient Egyptian papyri from the Roman period (circa 100 to 200 CE). Synchrotron-based macro–X-ray fluorescence (XRF) mapping brings to light the presence of iron (Fe) and lead (Pb) compounds in the majority of the red inks inscribed on 12 papyrus fragments from the Tebtunis temple library. The iron-based compounds in the inks can be assigned to ocher, notably due to the colocalization of Fe with aluminum, and the detection of hematite (Fe_2O_3) by micro–X-ray diffraction. Using the same techniques together with micro-Fourier transform infrared spectroscopy, Pb is shown to be associated with fatty acid phosphate, sulfate, chloride, and carboxylate ions. Moreover, micro-XRF maps reveal a peculiar distribution and colocalization of Pb, phosphorus (P), and sulfur (S), which are present at the micrometric scale resembling diffused "coffee rings" surrounding the ocher particles imbedded in the red letters, and at the submicrometric scale concentrated in the papyrus cell walls. A similar Pb, P, and S composition was found in three black inks, suggesting that the same lead components were employed in the manufacture of carbon-based inks. Bearing in mind that pigments such as red lead (Pb_3O_4) and lead white (hydrocerussite [$Pb_3(CO_3)_2(OH)_2$] and/or cerussite [$PbCO_3$]) were not detected, the results presented here suggest that the lead compound in the ink was used as a drier rather than as a pigment. Accordingly, the study calls for a reassessment of the composition of lead-based components in ancient Mediterranean pigments.

inks | ancient Egypt | papyri | synchrotron-based | microanalyses

Ink is history in the sense that ink has been used to inscribe a vast number of scripts and languages on various media over the course of more than 5,000 y. The earliest examples of preserving human thought by applying ink on a flexible and durable material, papyrus, are found in ancient Egypt at the dawn of recorded history (circa 3200 BCE). Black ink was employed for writing the main body of text, while red ink was often used to highlight headings, instructions, keywords, and so forth.

The general observation is that the ancient Egyptian black and red inks were made from organic and inorganic material, primarily soot and ocher, which was mixed with a binder, typically gum Arabic, and suspended in water, and at times perhaps in other fluids like animal glue, vegetable oil, and vinegar (1–3). The mixture was subsequently dried and pressed into pellets, which would be carried around by the scribe (4, 5) (*SI Appendix*, Fig. S15). A liquid ink could be prepared by mixing the pellet with a bit of water, when the scribe was ready to write a text using the nib of a reed pen. Thus, like in paints, the colorants employed by the ancient Egyptian scribes in inks can be classified as pigments rather than dyes, since they were always dispersed as solid and practically insoluble particles when applied to the writing surface (6). Although the original and continual employment of ink is in writing, it should be recalled that ink is also used in the delineation of objects by artists. Thus, ink and paint are mutually convertible to each other's uses and in ancient Egypt the verbs denoting "to write" and "to paint" (*sš*) were regarded as synonymous (1).

During the last decade many scientific studies have been conducted to elucidate the invention and history of ink in ancient Egypt and in the Mediterranean cultures, for example in ancient Greece and Rome. These studies have shown that at an early date novel black inks, such as copper- and lead-containing carbon inks,

Significance

Ink, invented in ancient Egypt circa 5,000 y ago, is the established and time-honored medium wherewith humankind commits words to writing. A comprehensive synchrotron-based microanalysis of a considerable corpus of ancient Egyptian papyri from the Roman period, inscribed with red and black inks, reveal a hitherto undetected complex composition of inks. Highlighted by the presence of iron, the red color can be attributed to the use of ocher. Unexpectedly, lead is regularly present in both the red and black inks and is associated to phosphate, sulfate, chloride, and carboxylate ions. The analysis shows that lead was probably used as a drier rather than as a pigment, similar to its usage in 15th century Europe during the development of oil paintings.

Author contributions: T.C., M.C., P.E.L., K.M., K.R., and S.L. designed research; T.C., M.C., V.G., P.E.L., K.M., K.R., and S.L. performed research; T.C., M.C., W.d.N., E.M., J.R.-H., S.d.M., F.V., N.S., and K.J. analyzed data; T.C., M.C., and S.L. wrote the paper; and T.C., M.C., N.S., V.G., P.E.L., K.M., K.R., and S.L. contributed to the theoretical discussion.

The authors declare no competing interest.

This article is a PNAS Direct Submission. K.F. is a guest editor invited by the Editorial Board.

[1]T.C. and M.C. contributed equally to this work.

[2]To whom correspondence may be addressed. Email: msc546@alumni.ku.dk or cotte@esrf.fr.

This article contains supporting information online at https://www.pnas.org/lookup/suppl/doi:10.1073/pnas.2004534117/-/DCSupplemental.

First published October 26, 2020.

were developed through continuous experimentation and used alongside charcoal/soot inks (7–20).

In contrast to the recently mapped history of black ink, the chemistry of red ink and the related painting and dyeing techniques is thought to be well known and has therefore received less attention. Previous analyses of the palette of colors in illustrated papyri—the so-called "Books of the Dead"—reveal that the source of the red ink in these papyri were, with rare exceptions, red ocher (hematite, Fe_2O_3) (21–23). Alternatively, the red color was derived from heated yellow ocher [goethite, FeO(OH)] rather than naturally occurring hematite (3).

In a recent work, we studied the red, orange, and pink inks inscribed on 11 fragments of 7 manuscripts from the only institutional library to survive from ancient Egypt, the so-called Tebtunis temple library (14). This exceptional library was discovered inside the main temple precinct at Tebtunis (modern Umm el-Breigât), located in the southernmost part of the Fayum depression some 100 km southwest of Cairo (*SI Appendix*, Fig. S16). The bulk of the library was found within two small cellars, where the manuscripts were deposited, when the temple was abandoned in the early third century CE. The manuscripts span the first through the early third century CE and rank among the most important assemblages of papyri unearthed in the sands of Egypt. The dry and brittle papyri are poorly preserved, and the material now consists of thousands of fragments from 400 to 500 manuscripts (24–26). The papyri selected for analysis were acquired in 1931 to 1938 by the Carlsberg Foundation on the antiquities market in Cairo (27). Today they are housed in the Papyrus Carlsberg Collection at the University of Copenhagen.

Our previous laboratory-based analyses revealed in a few cases a pink ink displaying UV-Vis spectra "vaguely resembling plant-derived anthraquinone pigment (i.e. madder lake)" (14). In most cases (~95%), X-ray fluorescence (XRF) point analyses revealed a regular use of a red ink based on a mixture of iron (Fe) and lead (Pb) compounds, undocumented in the analytical record. Fiber optics reflectance spectroscopy (FORS) supported the identification of ocher. However, none of the employed techniques—XRF, scanning electron microscopy-energy dispersive X-ray spectroscopy (SEM-EDXS), Raman spectroscopy, and FORS—could provide information about the nature of the lead-based compounds.

Hypotheses concerning the nature of this unique red ink can be inferred from ancient texts. For example, Pliny in his *Natural History* from the first century CE refers to a blend of red ocher that was calcined with lead white—that is, hydrocerussite $[Pb_3(CO_3)_2(OH)_2]$ and/or cerussite ($PbCO_3$)—to form a red-orange pigment called *sandyx*: "If ceruse (lead white) is mixed with red ochre in equal quantities and burnt, it produces *sandyx* or vermilion" (28). The pigment described by Pliny was employed as the flesh tone by Egyptian painters in the Roman period (circa 30 BCE to 400 CE) (29), but it has not been detected on papyri from ancient Egypt.

Moreover, minium—that is, red lead (Pb_3O_4), lead white, and other lead-based compounds (pigments and secondary products)—have been assigned to colors on ancient Egyptian objects, including inks on papyri, but also paintings on papyri, coffins, shrouds, mummy portraits, and so forth. Their occurrence and the techniques used for their identification are detailed in *SI Appendix*, Table S1. Minium was used in Egypt as early as the Second Intermediate Period (circa 1650 to 1550 BCE), incorporated into medicinal balms for stomach ailments (30). However, it came to be employed as a red pigment only in the Graeco–Roman periods (circa 332 BCE to 400 CE). Similarly, lead white was employed in cosmetics in Egypt at an early date, but only introduced as a colorant of objects in the Late (circa 664 to 332 BCE) and Graeco–Roman periods (21).

The introduction and production of these lead-based colorants in Egypt were likely influenced by Hellenistic and Roman painting techniques (29, 31). Both minium and lead white were used as principal colors, but also often mixed with other compounds—for example, hematite, goethite, cinnabar (HgS), calcite ($CaCO_3$), natrojarosite $[KFe_3(OH)_6(SO_4)_2]$—to produce different hues (*SI Appendix*, Table S1). Per se, lead-based pigments were thus employed by ancient Egyptian artists in a manner that is comparable to the use of "ceruse" (lead white) in the aforementioned red-orange pigment (*sandyx*) described by Pliny (28).

Objectives

The objectives of the present study were manifold: 1) To uncover the mineral compounds present in both red and black inks from the Tebtunis temple library and in particular to identify the nature of the iron and lead components utilized; 2) to evaluate the distribution of these compounds at the micrometer scale in order to acquire new insights into their origins; 3) to characterize white-black crusts forming on the surface of some of the red inks; and 4) to assess the composition of organic components present in the inks. Accordingly, we decided to revisit papyrus fragments from the Papyrus Carlsberg Collection using synchrotron radiation based macro- and μ-XRF, micro–X-ray diffraction (μ-XRD), and micro-Fourier transform infrared spectroscopy (μ-FTIR) techniques that can probe the chemical composition from the millimeter to the submicrometer scale and provide information not only on the elemental, but also the molecular and structural composition of the inks.

For a comprehensive description of methods and experimental set-up, see *SI Appendix*, *Methods*.

Methodological Approach

The studied corpus is exceptional, not only because the papyri derive from the Tebtunis temple library, but also because the present analysis includes as many as 12 ancient Egyptian papyrus fragments, all inscribed with red and black inks (Fig. 1 and *SI Appendix*, *Samples*). Accordingly, trends had to be extracted from 24 different samples of ink, which was challenging, considering the heterogeneity due to papyrus structure, ink composition, and ink degradation.

Intrasample heterogeneity was assessed at different scales by combining the information from the macro- and μ-XRF maps that we obtained on the surface of the papyri. Large fields-of-view and low-resolution macro-XRF maps were first acquired using a 50-μm or 100-μm diameter (∅) beam, whereas the beam was focused down to 0.4-μm vertical × 0.7-μm horizontal to assess at a micrometer scale the possible colocalization of elements present in the inks. To reduce the number of images shown and synthesize results, nonnegative matrix approximation (NNMA) analysis of the XRF data was performed (32, 33). NNMA analysis was carried out first on each macro-XRF fitted map. The number of components, which were between three and seven, was selected so that the main regions identified by visual observation of elemental maps (at least ink and edges around ink regions if any) were highlighted in the NNMA analysis. Then, all pixels (from macro- and μ-XRF maps) for each sample were decomposed on the basis of these vectors. The images shown in the figures below and in the supporting information in red, green, and blue (RGB) were chosen to highlight the components of interest.

To assess intersample heterogeneity and obtain a statistical overview of the composition of the 12 samples, we calculated 49 averages of XRF emissions of the principal elements present in the red and black inks and the papyrus fragments (Fig. 2*B*). For each macro-XRF map, a mask was obtained to attribute each pixel to ink (red or black) or papyrus. Masks were obtained based either on the NNMA analysis, the elemental maps, or visible images, when XRF maps did not exhibit any contrast. Subsequently, principal component analysis (PCA) was applied to the full dataset (Fig. 2*A*).

Results and Discussion

Macro- and μ-XRF principally detected sodium (Na), magnesium (Mg), aluminum (Al), silicon (Si), phosphorus (P), sulfur (S), chlorine (Cl), potassium (K), calcium (Ca), Fe, and Pb (Table 1 and *SI Appendix*, *X-Ray Fluorescence (XRF) Mapping* and Figs. S1–S11). The variations in the XRF intensity can mainly be attributed to the dissimilarities in the composition of the inks and the papyri, respectively, but in some instances also to variances in the thicknesses of one and the same ink; for example in sample 3, the difference between the XRF maps could be related to the

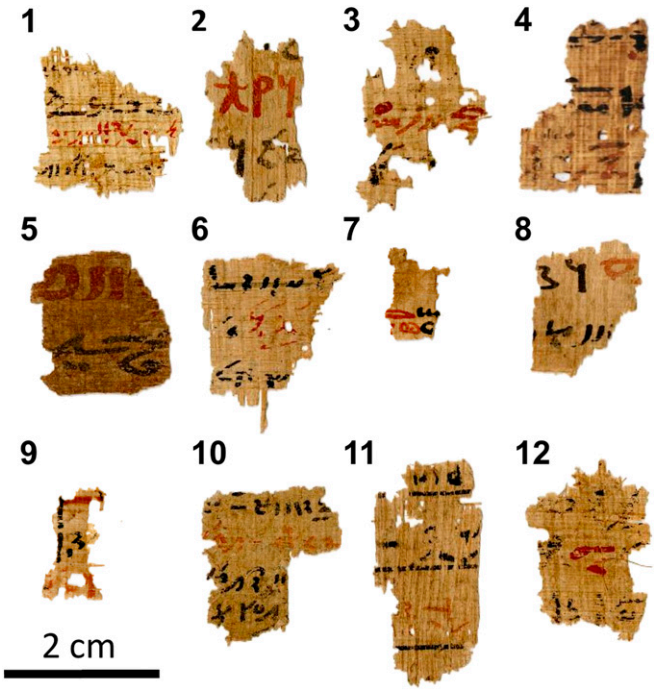

Fig. 1. Visible light pictures of the 12 samples with the sequential numbers assigned to them during the experiments written in bold (inventory numbers are listed in Table 1). The papyrus fragments derive from larger manuscripts from the Tebtunis temple library that are inscribed with both red and black ink: divinatory/astrological (samples 1, 2, 11), medical (samples 3, 6, 8, 9, 10, 12), and ritual (samples 4, 5, 7) texts.

different intensity of the red color in the two scanned letters and therefore to the concentration of the red pigment or the thickness of the ink layer (*SI Appendix*, *X-Ray Fluorescence (XRF) Mapping* and Fig. S2 *D* and *E*).

The penetration depth of the XRF K-line elements, such as Fe, is much higher than that of low Z elements and M-lines of Pb. The results presented here are therefore based on qualitative observations. Also, due to the high X-ray penetration, some elements present in the papyrus medium are also detected in the ink regions. Accordingly, the discussion on the ink composition below is based on the comparison of the XRF spectra in and out of the ink regions. Table 1 reports on the elements showing higher XRF intensity in the red and black inks than in the surrounding papyri.

General Analysis of the Average XRF Signals. Although both the red and black inks show considerable variation in their elemental composition, some trends can be observed clearly in the average XRF signals (Fig. 2 and Table 1).

In accordance to the trend observed with portable XRF point analysis (14), the majority (~95%) of the red inks contain Fe and Pb. Accordingly, the studied corpus can be considered representative of scribal practices at the library. More particularly, 10 samples of red ink (samples 1, 2, 3, 4, 6, 7, 8, 9, 11, and 12) contain Mg, Al, P, S, Fe, and Pb (Table 1). These red inks are distinguished from the papyri and black inks through the principal component 2 (PC2) axis (Fig. 2*A*). Furthermore, the red ink on samples 2, 4, 7, and 9 further stand out from the corpus due to a higher Pb XRF signal.

Red ink on sample 10, black inks, and papyri of most samples are located in the same central region showing that the contrast between the XRF signals for black inks and papyri is much less pronounced and that the red ink in question differs from the other samples containing rubricated words (Fig. 2*A*). Indeed, it does not contain Pb and also visually appears as a more vivid reddish orange color, when compared to the other red inks (*SI Appendix*, *Deviating Red Inks* and Fig. S9).

When plotting PC3 vs. PC2, a group of six points stands out from the rest of the corpus. They correspond to a single sample (sample 5). The composition of both inks, but also of the papyrus medium itself, differs from the other samples due to a significant contribution of P and S (Fig. 2*B*). Moreover, the red ink on the sample (sample 5) does not contain Pb and visually the papyrus appears darker. All of these features indicate that this papyrus probably does not belong to the Tebtunis temple library, or at least that the text had been written somewhere else (*SI Appendix*, *Deviating Red Inks* and Fig. S4). Some additional differences can be observed in the red inks containing Fe and Pb. In four samples (samples 2, 7, 9, and 12), Ca is more concentrated in the red ink than in the papyrus, and in samples 2 and 9 Si displays the same behavior.

Regarding the black inks, Pb was found in samples 1, 10, and 11 together with P and with S (*SI Appendix*, *X-Ray Fluorescence (XRF) Mapping*, and Figs. S1 *B* and *C*, S9 *E–H*, and S10 *E–H*). In sample 9, Mg, Al, Si, P, and Fe are more concentrated in the black ink (*SI Appendix*, *X-Ray Fluorescence (XRF) Mapping* and Fig. S8 *D–F*). In six samples (samples 4, 5, 6, 7, 8, and 12), no distinction could be made between the papyrus medium itself and the black inks on the basis of the XRF intensity of the elements excited in the present working conditions (no excitation of Cu in most of the XRF maps).

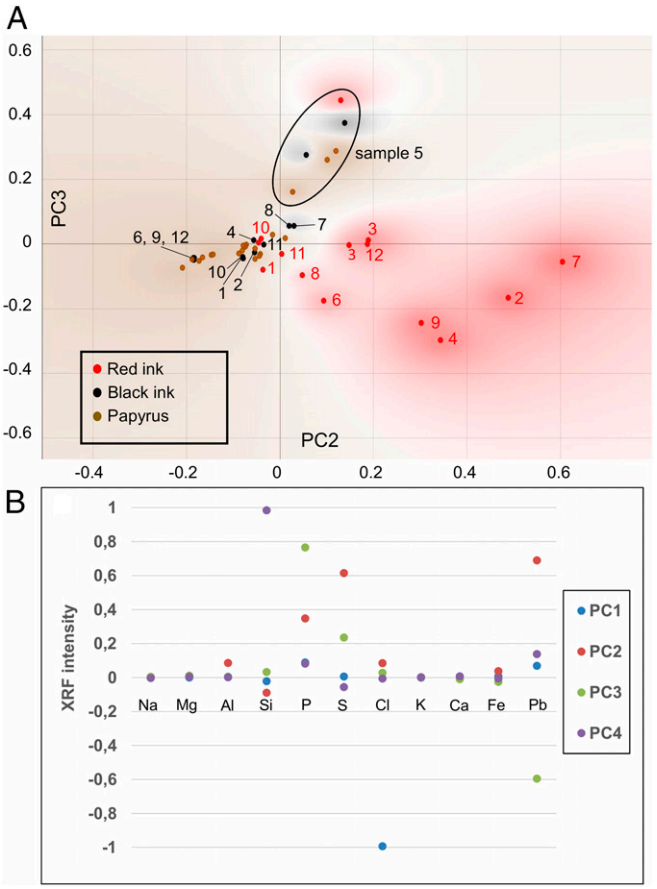

Fig. 2. PCA of 49 averages of the XRF elemental composition (macro-XRF maps; all samples labeled: "red", "black," and "papyrus"). (*A*) Scatter plot over the PC2 and PC3 axes. (*B*) XRF elemental intensity of the four PCs.

Table 1. List of the studied papyrus fragments

Sample no.	Inventory no.	Elements detected with macro-XRF	Elements associated with Fe in red inks (μ-XRF maps)	Elements associated with Pb in red inks (μ-XRF maps)	Other components detected in red inks (μ-XRF maps)
1	86	Red ink: Mg, Al, P, S, Fe, Pb (+Cu) Black ink: P, S, Pb (+Cu)	Al, P (finely dispersed)	P, S (diffused)	Few Ca particles (up to ~20 μm) in ink and papyrus; S also more concentrated in certain regions of ink, without correlation to another element
2	89	Red ink: Mg, Al, Si, P, S, Cl, K, Ca, Fe, Pb (Na, Ti, Ni). (+Cu) Black ink: No contrast	Mg, Al, Si, P, K (finely dispersed + some big (~20 μm) particles)	P, S (diffused and more concentrated at edges)	Ca, S particles (up to ~40 μm) Si particles (up to ~20 μm)
3	172	Red ink: Mg, Al, P, S, K, Fe, Pb (Mg, K, Ca, Ti, Mn) (+Cu) Black ink: No contrast (+Cu)	Mg, Al, P, S, K, Ca (finely dispersed)	P, S (diffused) At edges, the ratio Pb/(P, S) is higher (compare with vector 4 vs. vector 1 in *SI Appendix*, Fig. S3)	
4	SN 1	Red ink: Mg, Al, P, S, K, Fe, Pb (Mn, Co) Black altered regions in red ink: Mg, Al, Si, P, S, K, Ca, Fe White altered regions in red ink: Pb, Cl Black ink: No contrast	In red parts: Al, Si, K In black degraded parts: Mg, Al, Si, Ca, S, K (higher XRF intensity that in red)	P, S (diffused and at edges, transparent) In Cl (large white crystal aggregates in ink)	Ca particles in black parts (up to 30 μm) Si particles in black parts (up to 100 μm) NaCl particles on papyrus (up to 150 μm)
5	SN 2	Red ink: P, Fe (Ca, Mn) Black ink: P, Ca, Mg			
6	171	Red ink: Mg, Al, P, S, Fe, Pb (Co) Black ink: No contrast			
7	587	Red ink: Mg, Al, P, S, Ca, Fe, Pb (Ti, Mn, Ni, Co) Black ink: No contrast	Al (finely dispersed + some big (~50 μm) particles)	P, S (diffused at edges) Cl (large crystals aggregates in ink)	Ca, S particles (up to ~50 μm) Few Ca particles (up to ~10 μm) Si particles (up to ~50 μm) i n ink and papyrus
8	231 (13.2)	Red ink: Mg, Al, P, S, Fe, Pb (Ti, Mn) Black ink: No contrast	Al, P, S (finely dispersed + some big (~30 μm) particles)	P, S (diffused) Cl (large crystals)	Si particles (up to ~40 μm) and Ca particles (up to ~60 μm) in ink and papyrus
9	233 (3)	Red ink: Mg, Al, Si, P, S, Ti, Fe, Pb (Ca, Co) Black ink: Mg, Al, P, Si, (Fe)	Al, Mg, S, K (finely dispersed + few big (~20 μm) particles)	P, S (diffused)	Si particles (up to ~30 μm) and Ca particles (up to ~15 μm) in ink and papyrus
10	231 (13.1)	Red ink: S, (P, Al, Fe) Black ink: P, Pb, (S)		Black ink: P, S (diffused)	
11	101	Red ink: Al, P, S, Fe, Pb (Mg, S) Black ink: Al, Mg, P, S, Pb	Al, S (finely dispersed + few big (~10 μm) particles)	Both red and black inks: P, S (diffused)	Si particles (up to ~30 μm) and Ca particles (up to ~60 μm) in ink and papyrus
12	233 (4)	Red ink: Mg, Al, P, S, K, Ca, Fe, Pb (Ti, Co) Black ink: No contrast	(Fe, Al) finely mixed with (Ca, S) P and K diffused with both (Fe, Al) and (Ca, S)	P, S (diffused)	Ca particles (up to ~10 μm) in ink and papyrus

List of the studied papyrus fragments, which includes sample numbers, inventory numbers, and elements showing a higher XRF intensity in the red and black inks as compared to the surrounding papyri. In brackets, those elements for which the signal is low and/or alike to the one detected in the papyri are listed. Additional maps above Cu K-edge were acquired only for samples 1 to 4, and only in macro-XRF mode.

As shown in Fig. 2, the elemental composition in the papyrus medium itself is very similar in all of the fragments: Na, Mg, Al, Si, P, S, Cl, K, Ca, and Fe.

Assessing the Chemical Composition at the Micrometric Scale. Based on the macro-XRF results, a selection of nine representative samples of red ink containing Fe and Pb and two lead-containing black inks were studied further by μ-XRF. The discussion below is documented by the analysis of two samples: Samples 2 (Fig. 3) and 4 (Figs. 4 and 5), representative of the red inks containing Fe and high amounts of Pb. In addition, the results obtained for all samples are detailed in the supporting information (*SI Appendix*, *X-Ray Fluorescence (XRF) Mapping* and Figs. S1–S11). On sample 4, additional μ-XRD and μ-FTIR maps were acquired on the red ink to further investigate the ink composition and discoloration of the pigment. Visually, the pigment is of an orange-red color, while in other regions the surface of the ink exhibits white and black crusts (Figs. 4 and 5). Two μ-XRD maps were

acquired on each on these regions. Furthermore, tiny fragments were sampled in red nondamaged ink regions for μ-FTIR analysis.

The μ-XRF maps show clear (co)localization of some elements, notably in big crystals and in smooth regions over the red ink; the latter phenomenon characterizes especially the borders of the ink. It should be emphasized that Fe and Pb are not colocalized at the micrometer scale, but both are colocalized with some of the other elements. Table 1 summarizes the principal elements colocalized with Fe in the red inks and with Pb in the red and black inks, and the presence of additional particles. Their nature and origin are discussed in the subsequent paragraphs.

Papyrus Composition. In all samples, the papyrus fiber structure is emphasized at the macro scale by Si concentrated along parallel lines, as previously observed in studies of Egyptian and Greek papyri from Gebelein, Herculaneum, and Tebtunis (13, 15, 16) (*SI Appendix*, *X-Ray Fluorescence (XRF) Mapping*, and Figs. S4, S5, S10, and S11). Na, Mg, Al, Cl, K, and Ca are present throughout the papyri and are more concentrated in the holes defined by the Si structure (*SI Appendix*, *X-Ray Fluorescence (XRF) Mapping* and Fig. S11). The Si μ-XRF maps of the papyri sometimes highlight the rectangular cell structure of the papyrus (~20 × 25 μm^2), which are filled with Cl-containing spheres (~5- to 10-μm diameter) (*SI Appendix*, *X-Ray Fluorescence (XRF) Mapping* and Fig. S11). Moreover, the colocation of Na and Cl present as NaCl crystals all over the papyri (and the inks) is illustrated on two samples (sample 4 and 5) (*SI Appendix*, *X-Ray Fluorescence (XRF) Mapping*, and Figs. S3 and S4).

Iron-Based Compounds. In all of the samples, Fe is systematically found together with Al, sometimes also with Mg, Si, and K, as shown in the NNMA map for vector 2 obtained from sample 2 (Fig. 3). μ-XRD maps of the red ink on sample 4 reveal that Fe is primarily associated with hematite, which is responsible for the color of the ink (Fig. 5). Interestingly, in the map acquired on a less-degraded region a mixed copper iron sulfide ($Cu_xFe_yS_2$) was also detected and is colocated with the hematite. The most common of these minerals is chalcopyrite ($CuFeS_2$), but this mineral did not match well with the XRD data. Thus, the exact stoichiometry of this phase could not be determined. This compound is believed to be an impurity found together with hematite. Regarding its distribution, Fe is usually present as a mixture of fine particles (smaller than the pixel size) and larger particles (some tens of microns), corresponding to a fine or raw grinding of ocher, respectively, and its distribution follows the red color perfectly. The additional elements detected besides Fe in the red pigments (Al, Mg, Si) can be attributed to impure ocher deposits containing a mixture of mineral components, such as sand, clay, quartz (SiO_2), or alumina (Al_2O_3) (34).

It should be noted that Cu was not excited in most of the present XRF acquisitions, except for additional maps acquired on three samples of red and black ink (samples 1, 2, and 3) and only at low resolution. These measurements show that Cu is more concentrated in one black ink (sample 3) and in the three red inks (*SI Appendix*, *X-Ray Fluorescence (XRF) Mapping* and Fig. S12). As previously observed in our study of four ancient Egyptian copper-containing carbon-black inks from the Papyrus Carlsberg Collection, Cu follows the papyrus fiber structure as well (13). This result warrants further study, since it shows that Cu is not specific to black inks.

Lead-Based Compounds. Conversely to Fe, Pb does not exhibit a pigment particle distribution. In all of the studied samples (nine red inks and two black inks), it is colocalized with P and S in a

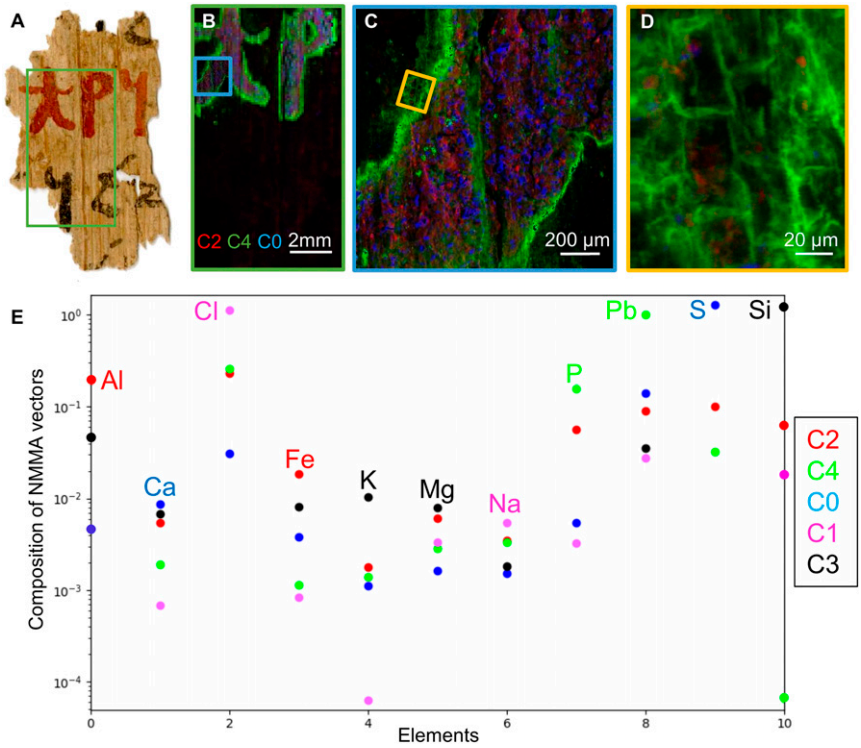

Fig. 3. Macro- and μ-XRF mapping of sample 2. (*A*) Visible light image of the sample. (*B–D*) Macro- and μ-XRF maps including RGB maps of NNMA vectors 2, 4, and 0. (*B*) Macro-XRF map (green rectangle). E = 3.0 and 9.0 keV. Beam size: 100 μm ∅. Area size: 12.4 mm horizontal × 6.9 mm vertical. Step size: 100 μm horizontal × 100 μm vertical. (*C*) μ-XRF map (blue rectangle in *B*). E = 3.0 and 9.0 keV. Beam size: 0.7 μm horizontal × 0.7 μm vertical. Area size: 1.316 mm horizontal × 1.296 mm vertical. Step size: 4 μm horizontal × 4 μm vertical. (*D*) μ-XRF map (yellow rectangle in *C*). E = 2.9 and 8.7 keV. Beam size: 0.54 μm horizontal × 0.75 μm vertical . Area size: 140 μm horizontal × 140 μm vertical. Step size: 0.7 μm horizontal × 0.7 μm vertical. (*E*) NNMA vectors obtained from *B* (green rectangle in *A*).

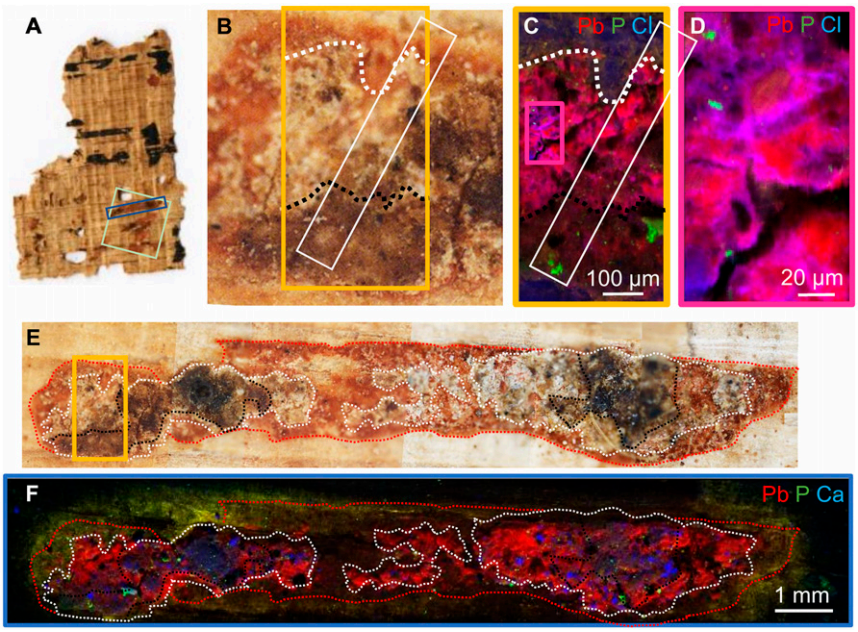

Fig. 4. µ-XRF mapping of sample 4. The red, white, and black dotted curves highlight the red ink, the white, and black debased areas, respectively. (*A*, *B*, and *E*) Visible light images of the sample. The yellow and blue rectangles inserted in the images highlight the areas scanned by µ-XRF (*C* and *F*, respectively). The light green rectangle highlights the area scanned by macro-XRF as shown in *SI Appendix, X-Ray Fluorescence (XRF) Mapping* and Fig. S3. (*B*) Visible light image of (*C*) µ-XRF map of black and white debased areas (yellow rectangle), and RGB maps of Pb, P, and Cl. E = 2.9 keV. Beam size: 1 µm horizontal × 1 µm vertical. Area size: 350 mm horizontal × 700 mm vertical. Step size: 2 µm horizontal × 2 µm vertical. The white rectangle shows the area scanned by µXRD/µXRF (Fig. 6). (*D*) µ-XRF map, including RGB maps of Pb, P, and Cl, which detail the composition of the white crystals. E = 2.86 keV. Beam size: 1 µm horizontal × 1 µm vertical. Area size: 90 mm horizontal × 160 mm vertical Step size: 1 µm horizontal × 1 µm vertical. (*E*) Visible light image of (*F*) µ-XRF map (blue rectangle) including RBG maps of Pb, P, and Ca. E = 4.045 KeV. Beam size: 1 µm horizontal × 1 µm vertical. Area size: 5.908 mm horizontal × 1 mm vertical. Step size: 2.5 µm horizontal × 10 µm vertical.

material diffused all over the ink lines. In seven samples of red ink (samples 1, 2, 3, 4, 6, 7, and 12), Pb, P, and S are more concentrated on the edges of the ink lines, forming a kind of halo around the iron-rich lines; see, for example, the map of the NNMA for vector 4, obtained from sample 2 (Fig. 3), and of the NNMA for vector 5 obtained from sample 4 (Fig. 4 and *SI Appendix, X-Ray Fluorescence (XRF) Mapping* and Fig. S3). Under the visible microscope, this halo appears in a lighter orange halo surrounding the red ink, and in some regions, it is invisible. In five samples (samples 2, 7, 8, 11, and 12), detailed maps have revealed that Pb, P, and S cover the walls of the papyrus cells (Fig. 3 and *SI Appendix, X-Ray Fluorescence (XRF) Mapping*, and Figs. S6, S7, S10, and S11). A similar halo has been observed on a SEM image of a black ink on a Greek papyrus fragment (circa 100 to 200 CE) from Tebtunis (8). The single-point EDXS spectrum in that study revealed the presence of mainly Si, P, Cl, Ca, and Pb (S was not mentioned but is probably overlapping with the Pb M-line signal). Furthermore, Pb, P, Cl, and possibly S were found colocalized and diffused in the black inks inscribed on carbonized papyrus fragments from Herculaneum (15, 16).

Lead phosphate compounds. The colocalization of Pb and P can be associated to the presence of a calcium-lead phosphate compound, which was detected with µ-XRD (Fig. 5). Phosphohedyphane ($Ca_{1.838}Pb_{3.162}[PO_4]_{2.7271}[AsO_4]_{0.279}Cl$) was the phase automatically identified by comparison with the Crystallography Open Database. However, the broad signals, probably due to a semicrystalline or nanocrystalline compound, could possibly also be assigned to other Ca-Pb phosphates of a generic formula ($[Ca, Pb]_5[PO_4, AsO_4]_3[Cl, OH]$). As shown by the elemental maps of Pb vs. Fe in the red inks, lead phosphates disperse from the hematite/red pigment but are not visible under an optical microscope (Figs. 4 and 5).

The origin of the detected lead phosphates (original or degradation product, synthetic or natural) is unclear. Only a few studies report on the presence of lead (calcium) phosphates in ancient Mediterranean archeological and artistic contexts. It has been suggested that hydroxypyromorphite [$Pb_5(PO_4)_3OH$] detected on Roman wall paintings, together with red ocher, could be due to the intentional use of mineral pyromorphite [$Pb_5(PO_4)_3Cl$] instead of lead white in the preparation of the pigment *sandyx* (35). Pyromorphite has also been reported in early Islamic pigments at Nishapur, northeastern Iran, and an imported geological source for the mineral was hypothesized (36). Other studies associate (calcium) lead phosphates to degradation, for example the interactions of a metallic alloy of a buried Roman bronze inkwell with residues from agricultural fertilizers and soil amendments (37), and the reaction of hydroxylapatite [$Ca_5(PO_4)_3(OH)$] with litharge (PbO), cerussite, or other lead compounds in tools employed for the preparation or use of lead-based pigments at Akrotiri, Greece, during the Cycladic Bronze Age (circa 3000 to 1600 BCE) (38).

In the specific context of inks and pigments dating to the Roman period, it is noteworthy that metallic phosphates have been reported in pigments from Pompeii directly sampled in vessels: 1) In six black powders, sampled in bronze vessels (however, the authors do not state if they are phosphates of calcium and/or lead) (18); 2) in a reddish white pigment and in a light gray pigment, both sampled in bone pyxides (39); 3) in two glass *unguentarii*, where whitlockite [$Ca_9(Fe,Mg)(PO_3OH)(PO_4)_6$] and phosphohedyphane were clearly identified (17). Except in the case of bone vessels, where phosphates may originate from the container, the many occurrences of Pb and P (and occasionally S) in inks from the Roman period suggest that they result from a precise and regular formulation, rather than an accidental presence. Moreover, their association in many black inks from the ancient Mediterranean supports that they were added into the ink composition in order to better bind the pigment, whether black or red, rather than to enhance the color.

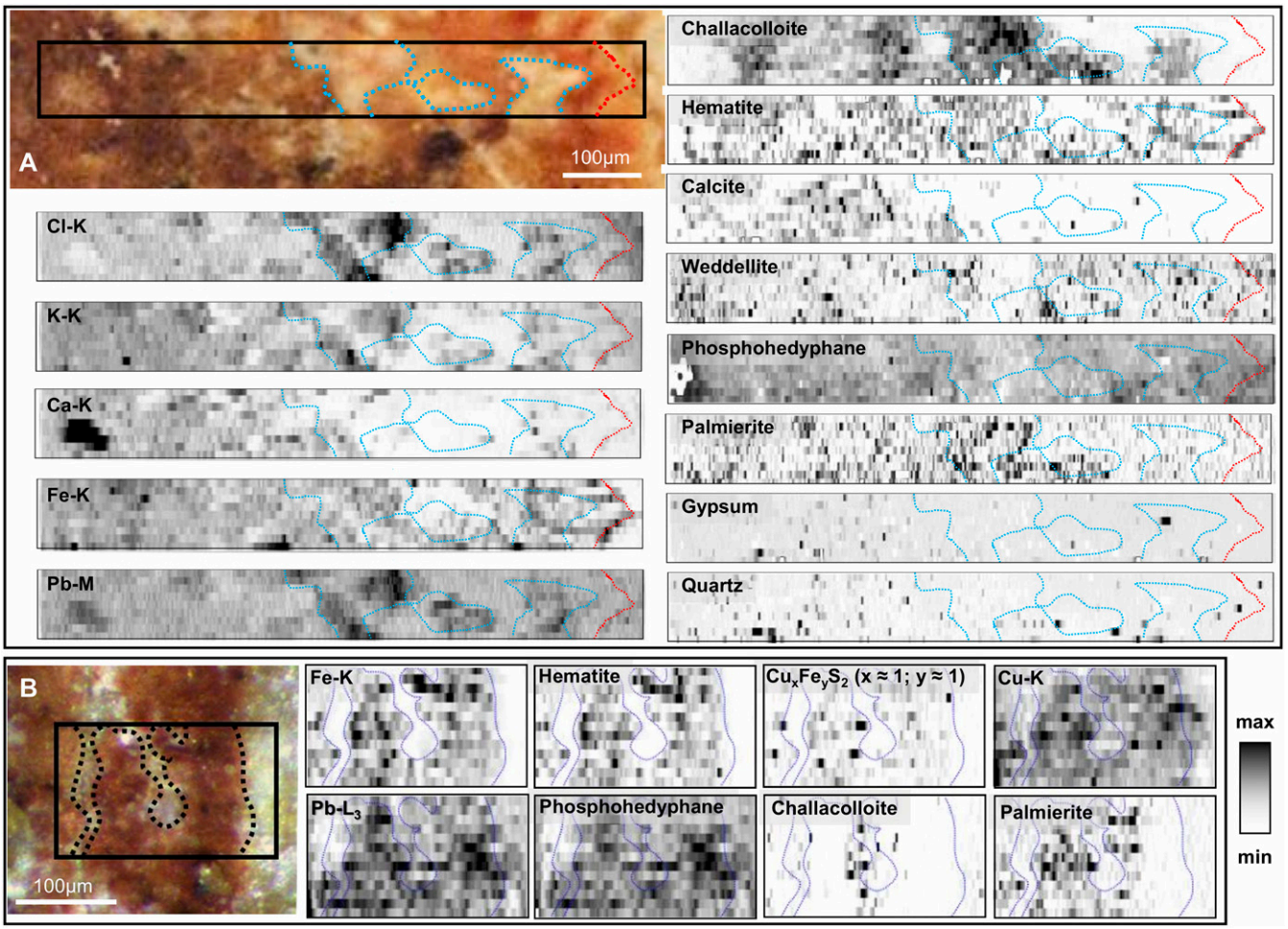

Fig. 5. Visible light images, elemental and crystalline phase maps of red ink on sample 4. The location of the two maps and the identification of the main crystalline phases are shown in *SI Appendix, X-Ray Diffraction (XRD) Mapping*, and Figs. S13*A* and S14. (*A*) Maps acquired on a white/black debased region on the red ink. The red dotted lines highlight the edge between red ink and papyrus (compare with Fe and hematite distribution). The blue dotted lines highlight the white crystals (compare with Cl, K, Pb, and challacolloite distribution). E = 8.53 keV. Beam size: 1 μm horizontal × 1 μm vertical. Area size: 765 μm horizontal × 100 μm vertical. Step size: 2.5 μm horizontal × 10 μm vertical (ID21, European Synchrotron Radiation Facility). (*B*) Maps acquired on a non-degraded red region. The black dotted line highlights the edge between red ink and papyrus (compare with Fe and hematite distribution). E = 14 keV. Beam size: 2 μm horizontal × 2 μm vertical. Area size: 238 μm horizontal × 120 μm vertical. Step size: 2.5 μm horizontal × 10 μm vertical (I18, Diamond Light Source). In the gray scale of μ-XRF and μ-XRD maps, darker pixels correspond to higher intensities. Additional maps and XRD patterns are show in *SI Appendix, X-Ray Diffraction (XRD) Mapping* and Figs. S13*B*.

As an alternative to the hypotheses of natural or degradation origins, the possibility that lead phosphates were synthesized intentionally should receive more consideration. Fundamentally, their presence does not affect the readability of the papyri and indeed they could have a "self-consolidating" role, which hardens the ink layer (40). Except in the case of bone vessels, where phosphates may originate from the container, the many occurrences of Pb and P (and occasionally S) in inks from the Roman period suggest that they result from a precise and regular formulation, rather than an accidental presence. Moreover, their association in many black inks from the ancient Mediterranean supports that they were added into the ink composition in order to better bind the pigment, whether black or red, rather than to enhance the color. It has been demonstrated that, in acidic aqueous solutions, hydroxypyromorphite $[Pb_{10}(PO_4)_6(OH)_2]$ forms in 2 d through the reaction of hydroxyapatite with PbO or $PbCO_3$ (41). To our knowledge, such a reaction has only been studied in aqueous solutions, but the reported vulnerability of bone-black pigments in oil paintings in the presence of a lead catalyst provides an initial insight into the possible occurrence of such a reaction in an organic medium (42).

Lead sulfate compounds. Pb and S also exhibit colocalization down to the submicrometric scale. μ-XRD detects palmierite (K_2PbSO_4). This phase is more concentrated in the debased region of red ink but is also detected in the visibly nondegraded red ink (Fig. 5). Its distribution cannot be associated to a specific color and it may be present as a transparent film. Indeed, various lead sulfates—palmierite but also anglesite ($PbSO_4$) and lanarkite $[Pb_2(SO_4)O]$—have already been reported as degradation products in paintings, where they usually form a transparent film and sometimes protrusions (43–46). They were detected in Old Master Paintings and associated with colored pigments (e.g., smalt and lakes) in combination with lead white that is present in the same or an adjacent paint layer. Similarly, to the formation of gypsum from lime or calcite, the formation of lead sulfate is generally ascribed to the reaction of lead pigments or driers (e.g., minium and PbO) with environmental SO_2 (47). Closer to the subject at hand, it should be noted that palmierite and anglesite were detected in four ancient Egyptian lead-based make-ups dated

between 2000 and 1000 BCE (48). Moreover, anglesite was detected in one of the six Pompeian black powders mentioned above (18). Again, as for the phosphates, the pertinent question is whether the lead sulfates were present in the inks originally or rather were formed subsequently through the interaction of a lead compound with SO_2 from the air or sulfate from the soil in which the papyri were found.

Lead chloride compounds. μ-XRF maps show for three samples of red ink (samples 4, 7, and 8) aggregation of crystals containing Pb and Cl (Fig. 4 *B–D* and *SI Appendix*, *X-Ray Fluorescence (XRF) Mapping*, and Figs. S6 and S7). In two samples (samples 4 and 7), the presence of Pb and Cl can clearly be related to white/gray crystals, dispersed over the surface of the red inks. Accordingly, they can conclusively be associated to a degradation product, since these crystals affect the rendering of the red ink. Additional μ-XRD maps on the black and white crusts reveal the presence of challacolloite (KPb_2Cl_5) or the structurally closely related compound $NH_4Pb_2Cl_5$ (Fig. 5). In contrast to the μ-XRF map of Cl and Pb, the detection of this phase in the black crust suggests that the white crystals are probably also present beneath the dark-gray crust (detected in transmission-XRD, while Cl K-lines and Pb M-lines may be reabsorbed by the gray crust).

Challacolloite was previously identified with XRD in the pigment palette of contemporary Roman portrait paintings, also excavated in Tebtunis (49), and in blue (with Egyptian blue and calcite), white (with calcite), pink (with hematite), and green (with Egyptian blue and goethite) pigments in paintings on a Ptolemaic *Book of the Dead* papyrus (22) (*SI Appendix*, Table S1). This compound is believed to be formed in situ in a potassium- and chloride-rich environment from the reaction of hydrocerussite with KCl (22). This hypothesis was supported by the μ-XRD maps of challacolloite and hydrocerussite over a cross-section of a fragment of a Roman mummy portrait from Tebtunis, where the distribution of challacolloite appears at the paint surface and complementary to that of hydrocerussite (49).

It is important to note that investigations into the soil of the Fayum province, undertaken as early as 1902, demonstrated that the soil in the area where the papyri were found is especially high in salt (also illustrated by the presence of NaCl at the surface of some papyri, notably sample 4) (50, 51). These studies showed that the soil contained sodium chloride and sodium sulfate at concentrations up to 5.3%. The analysis concluded that the irrigation water in the Fayum was not the source of the salt, but rather the desert sand, and the underlying limestone and clays. Therefore, a chemical reaction, similar to the one outlined for challacolloite above, between a lead compound in the red inks and chloride and potassium from the environment in which the papyri were found, seems very plausible.

Lead carboxylates. The unique distribution of Pb, P, and S around the red letters similar to "coffee rings residues" (52) in almost half of the samples of red ink suggests that Pb was present in the inks in a finely dispersed form or even dissolved in the binder, and would have diffused with the binder during application of ink onto the papyrus. To assess this hypothesis and identify the nature of such a binder, additional μ-FTIR maps were acquired on sample 4. Unfortunately, μ-FTIR could not be performed non-invasively directly on the papyrus fragment, and very tiny fragments (~200 μm) were gently detached in a region where the red ink was flaking away. Sample preparation was very challenging, and it was impossible to selectively sample ink without papyrus due to the thorough penetration of ink into the papyrus fibers. Accordingly, most of the FTIR spectral features are ascribed to papyrus absorption. To avoid contamination from any embedding medium, the fragments were simply flattened between two diamond cells, which affects the readability of the visible image and FTIR maps significantly. However, by exploiting simple regions-of-interest peak intensity mapping and NNMA analysis, we succeeded in attributing small FTIR peaks to additional minor compounds (Fig. 6).

In Fig. 6, the main component (vector 0) corresponds to the papyrus signal. Vector 2 exhibits absorption bands attributed to clay (sharp O-H stretching peaks at 3,696 and 3,622 cm^{-1}), calcium oxalate (carbonyl stretching band at 1,318 cm^{-1} and broad antisymmetric carbonyl stretching band at 1,662 cm^{-1}), and calcium sulfate [ν_3 $(SO_4)^{2-}$ stretching vibration at 1,131 cm^{-1}]. The peak at 970 cm^{-1} can possibly be ascribed to lead phosphates; however, this peak shows a high overlap with an intense absorption of papyrus, which makes the identification and mapping of lead phosphates delicate. The map of CH stretching (2,800 to 3,000 cm^{-1}) highlighted the diffused presence of aliphatic hydrocarbons. The nature of this organic phase is difficult to identify, since the fingerprint area (1,750 to 700 cm^{-1}) overlaps with cellulose and

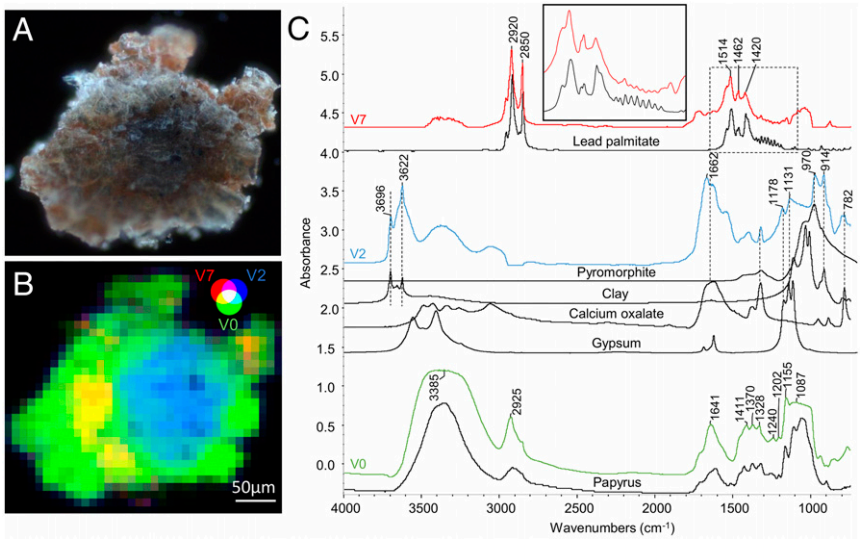

Fig. 6. μ-FTIR mapping on a section from sample 4. (*A*) Visible light image of the sample. (*B*) RGB display of 3 NNMA vectors from the FTIR map (red = V7; green = V0; blue = V2). Beam size: 20 μm horizontal × 20 μm vertical. Area size: 380 μm horizontal × 330 μm vertical. Step size: 10 μm horizontal × 10 μm vertical. (*C*) NNMA components superimposed on spectra of reference materials: Lead palmitate, pyromorphite, clay (kaolinite), calcium oxalate, gypsum, papyrus (average spectrum acquired on a section of sample 4 far from the ink region).

hemicellulose absorptions. Consequently, it is quite remarkable that lead carboxylates were sufficiently concentrated in a few pixels to be identified (vector 7). More particularly, the band progression in the region 1,360 to 1,200 cm^{-1} (see *Inset* in Fig. 6*C*), assigned to wagging and twisting-rocking vibrations of methylene groups, allows for the unequivocal identification crystallized lead palmitate [$Pb(C_{16}H_{31}O_2)_2$].

The presence of lead carboxylates was already proposed, but without sufficient experimental evidence, in the black ink on carbonized papyrus fragments from Herculaneum (15, 16). This hypothesis was supported by Pb K-edge X-ray absorption near edge structure spectroscopy, and by previous identification of lipids of animal and/or plant origin in nine black powders excavated in houses in Pompeii, likely used as both inks and cosmetics (18). In a recent publication, the analysis of a set of ancient Egyptian papyrus fragments highlighted the presence of aliphatic hydrocarbons (FTIR imaging) together with the presence of Pb (SEM-EDXS) in a black ink inscribed on a Greek papyrus (circa 300 to 400 CE) from Antinoë (*SI Appendix*, Fig. S16). However, the detection of lead carboxylates is not discussed in this study (8). Recently, lead carboxylates have been detected by μ-FTIR in an almost "invisible" ink inscribed on an Egyptian papyrus from Elephantine (*SI Appendix*, Fig. S16) that dates to the Graeco–Roman periods (circa 332 BCE to 250 CE). The authors of this study note that "its deliberate use as an ink for encryption seems very unlikely" (9). Our unequivocal detection of lead carboxylates in ancient Egyptian inks show that they probably were produced and used intentionally.

When vegetable oil is mixed with litharge, the immediately formed lead carboxylates acquire excellent drying properties (53). These qualities inherent in lead carboxylates were fundamental for the development of the oil painting in Europe in the 15th century. However, already in Antiquity the drying properties of lead oxide and lead white were known and exploited (54). Indeed, the use of litharge as an oil drier was mentioned by Galen and Marcellus in the second and fourth centuries CE, respectively (53, 54). Moreover, litharge together with quicklime are employed in four formulae for dyeing preserved in a Greek alchemical papyrus, dating to the third century CE (55, 56). In addition to dyeing techniques, the manuscript discusses the manipulation of metals, the counterfeiting of precious stones, and the manufacturing of silver and gilded inks. It was found in Thebes (*SI Appendix*, Fig. S16), and it may well have belonged to a priestly library (57) like the papyri studied here, thus providing insights into some of the chemical arts applied by Egyptian priests of the late Roman period.

Lead-based driers prevent the binder from spreading too much, when ink or paint is applied on the surface of paper or papyrus (58). Indeed, in the present case, Pb forms an invisible halo surrounding the ocher particles. When mixed with oil lead oxide rapidly dissolves and is no longer detected by XRD (59). This could explain that while the use of litharge is reported in historical texts, to date it has not been detected in ancient Egyptian pigments.

Interestingly, lead carboxylates have also been identified in ancient Egyptian cosmetics from early New Kingdom (circa 1550 to 1300 BCE) (60). Moreover, striking correspondences can be established between the composition of red inks studied here and medicinal balms recorded in ancient Egyptian medical papyri. An example is provided by the following formula inscribed on a papyrus dating to circa 1550 BCE: "Another (remedy) for treating the eyesight; galena 1, red ocher 1, carob (juice) 1, *gesefen* 1, male part of galena 1. Prepare as a single substance and apply to the eyes" (61). The word typically translated as "galena" (ancient Egyptian: *msdmt*) did not have a precise chemical definition and could be applied in general to lead-based and related mineral substances used in eye-paint (62). The meaning of *gesefen* remains uncertain, although it has been equated with manganese oxide (63).

Calcium-Based Compounds. In addition to Fe and Pb compounds, other minerals were detected. Macro-XRF on four samples (samples 2, 4, 7, and 12) shows a higher concentration of Ca and S in the red ink, while μ-XRF reveals that in two of these samples (samples 2 and 7) large crystals (up to 50 μm) containing Ca and S are present (see NNMA map of vector C0 in Fig. 3 and *SI Appendix*, *X-Ray Fluorescence (XRF) Mapping*, and the NNMA map of vector C3 in *SI Appendix*, Fig. S6). In one of the samples (sample 12), these particles are also detected, but more intimately mixed with the iron-based pigment (*SI Appendix*, *X-Ray Fluorescence (XRF) Mapping*; see NNMA map of vector C4 in *SI Appendix*, Fig. S11). In sample 4, Ca and S are primarily colocalized in black debased areas (*SI Appendix*, *X-Ray Fluorescence (XRF) Mapping* and Fig. S3 *C* and *D*) and can be associated to gypsum ($CaSO_4{\cdot}2H_2O$) as identified by μ-XRD (Fig. 5). Furthermore, particles containing Ca, but not S, are found in the red inks of three samples (samples 5, 9, and 12), in degraded areas of sample 4 and all over the papyri (not specific to ink) in three further samples (samples 7, 8, and 11). Based on μ-XRD analyses, it is likely that in sample 4, these particles can be attributed to calcium carbonate (calcite) and hydrated calcium oxalate weddellite ($CaC_2O_4{\cdot}2H_2O$). The calcite distribution clearly fits with the black crust, while weddellite cannot be associated to a particular color and is detected outside of the red ink as well (Fig. 5).

Calcite and gypsum were occasionally added as a toner in red pigments from Egyptian painting workshops (22, 64) (*SI Appendix*, Table S1). Together with quartz, they were also detected in two studies of Pompeiian carbon blacks (17, 18) and gypsum was the main component of six further Pompeian black inks (39). Thus, calcite and gypsum could have been used not only to modify the red color, but also as ink-driers (17). However, the calcium-containing compounds detected on sample 4 are most likely degradation products, since calcite and gypsum are concentrated in the tainted areas, even if the latter is also detected in the red ink. This distribution, as well as the higher concentration of Fe, Al, Si, and K in these areas recall black crusts observed on debased cinnabar paintings found in the vicinity of Pompeii (65). Accordingly, calcium sulfate would be a secondary product in this particular sample, presumably formed from a reaction of environmental or internal sulfates with calcite, which would have trapped dust and thereby creating a gray/black film upon the surface of the ink. Moreover, weddellite, and oxalates in general, are frequently found as degradation products in paintings (42, 44) but also in stones (66), and even on the skin of ancient Egyptian mummies (67).

Silicon-Based Compounds. Samples 2 and 4 show higher Si XRF intensity in the red inks. Quartz was indeed detected by μ-XRD in sample 4 (Fig. 5). Si was also detected in the black ink of sample 9 as large particles (30 μm) associated with Al, Fe, and Mg in finely dispersed ~20-μm particles (*SI Appendix*, *X-Ray Fluorescence (XRF) Mapping* and Fig. S8). This suggests that quartz and ocher is also present in the black ink of this sample. As mentioned above, quartz was detected in two studies of Pompeiian carbon blacks (17, 18). Silicon-containing crystals were also observed in samples 7, 8, and 11, but not specifically in the inks, which suggest that they derive from the environment in which the manuscripts were found.

Conclusions and Outlook

Thanks to noninvasive X-ray microscopy analysis of a large corpus of 12 red and 12 black inks inscribed on papyri from the only institutional library to survive from ancient Egypt, clear representative trends could be observed in relation to ink manufacturing in a community of literate priests. Concerning the latter, our study confirms and further extends on the recent works on the composition of black inks from the ancient Mediterranean cultures. Concerning the former, their color can be attributed to the use of ocher as highlighted by the presence of Fe in 11 of the 12 red inks and the detection of hematite. Calcite, quartz, and gypsum were also detected in these inks, but in a less systematic manner. Only in

one instance does the absence of metals and the presence of sulfur suggest the use of an organic pigment in a vivid red-orange ink (*SI Appendix*, *Deviating Red Inks* and Fig. S9).

Unexpectedly, Pb is regularly present in the inks, not only in the black inks (3 of 12 samples), but also in red inks (10 of 12 samples). Surprisingly, the lead-based compounds most commonly employed as pigments in the ancient Mediterranean cultures (i.e., minium and lead white) were not detected. Instead, a complex mixture of lead phosphates (presumably phosphohedyphane), potassium lead sulfates (palmierite), lead carboxylates (more particularly crystallized lead palmitate), and lead chlorides (presumably challacolloite) was identified using μ-XRF, μ-XRD, and μ-FTIR. While the lead chlorides can clearly be associated with white secondary crystals forming a crust on the red ink, the three other compounds cannot be seen in visible light and determining their origins is by no means straightforward. Basically, three sources for Pb, S, P, and fatty acids should be considered: The papyrus, the environment, and the ink.

P, S, and fatty acids are naturally present in plant cells and it is known that when exposed to metals, phytochelatins and metallothioneins can chelate to metal ions through thiolate functional groups, giving rise to a higher local concentration of S and metals (68), which in turn could explain the peculiar distribution and colocation of Pb and S in the cell walls of the papyri. However, this thiolation occurs in living plants and model experiments would be needed to investigate if Pb can affix S (and P and fatty acids) in dried and manufactured papyrus sheets as well.

The possible degradation of original lead-based pigments or driers by exposure to P and S from the environment—akin to the formation of the potassium lead chloride crystals—also deserves consideration, since analogous chemical alterations are often reported in relation to aged paintings (47). Considering the significant amount of not only K and Cl, but also P and S present in Egyptian desert soil (69), it is possible that, for example, minium was originally present in the inks and later degraded into the different lead compounds that we have detected. However, such interactions usually require prolonged exposure to humidity, which is detrimental to the survival of ancient papyrus manuscripts. Accordingly, further experiments are needed to assess this hypothesis, in particular studies of soil samples from the archaeological layers in which the papyri were found.

The presence of Pb in the inks on the papyri has been convincingly demonstrated, since Pb would not be present solely in the inked areas, if it derived from the papyrus or the environment. The fact that no lead-based pigment is detected and that Pb is present in both red and black inks supports the hypothesis that lead compounds were used for their drying properties (rather or not only for their color), just as they were in 15th century Europe during the development of the oil painting. In addition, in the same period, the Italian painter Cennino d'Andrea Cennini (circa 1360 to 1427 CE) gives advice for the preparation of parchments and recommends the use of calcined bone, lead white, and oil as a coating (70). Modern day reproductions of such historical recipes would be needed to assess the formation of lead calcium phosphates over time. As for the original lead compounds used in the inks, lead oxides and minium can be hypothesized, since—because of their alkalinity—they have a higher tendency to saponify fatty ester (71), which could explain the presence of lead carboxylates in the inks.

Accordingly, credit should also be given to the hypothesis that lead sulfates, phosphates, and/or carboxylates were present in the inks before they were applied onto the papyrus medium, since as specified above, anglesite, phosphohedyphane, and lipids of animal and plant origin have been identified in carbon black pigments from Pompeii that were employed either as inks or cosmetics (17, 18). The distribution of Pb at the edges of red ink indicates that Pb was either dissolved in the ink or was present in much smaller particles than hematite. The coffee ring phenomenon could have separated large hematite particles from some of the lead-based particles (72). The presence of Pb, P, and S in the inks—colocalized at the submicrometric scale and concentrated in the cell walls of the papyri—can be explained in various ways. Either Pb, P, and S were already solubilized in the inks and were deposited on the cell walls when applied onto the papyri, or dissolution and recrystallization of lead phosphates and sulfates later led to the formation of a film that covered the cell walls.

Considering the complex composition of the bulk of red inks analyzed here—and the amount of raw materials needed to supply a temple library—it seems unlikely that the priests, who wrote the manuscripts, manufactured the inks themselves. Rather, they must have acquired them or overseen their production at specialized workshops much like the Master Painters from the Renaissance. As such, it is important that a magical spell inscribed on papyrus, which was found together with the abovementioned alchemical treatise, refers to a red ink that was prepared inside a workshop (Greek: ἐργαστήριον) (1).

The results presented in this article have provided valuable information on the preparation and composition of red and black inks in ancient Egypt and Rome circa 2000 y ago. The red color was mainly obtained by ocher. Lead compounds were detected in most red inks and some black inks and their distribution supports that they were probably employed for their drying properties rather than for coloring ink. To complete the picture of the composition of these novel historical inks, supplementary experiments are required. For example, an evaluation of the reactivity (deliberate or accidental, fast or slow) of lead compounds such as lead white and lead oxide with hydroxyapatite in an organic medium—as already observed in aqueous solutions (41)—is warranted. Such an assessment could explain the formation and presence of lead(-calcium) phosphates in historical inks and paints. Moreover, the detection of potassium lead chloride in white/gray crystals at the surface of some red inks also calls for further studies of the degradation of lead compounds, which will facilitate future strategies of conservation and preservation of cultural heritage objects.

Data Availability. All study data are included in the article and supporting information.

ACKNOWLEDGMENTS. The research was conducted as part of the project University of Copenhagen Neutron and X-ray Techniques (CoNeXT; S.L. Principal Investigator) under the University of Copenhagen Excellence Programme for Interdisciplinary Research (https://chem.ku.dk/research_sections/finished-projects/conext-temporary/). The authors thank the European Synchrotron Radiation Facility for granting beamtime at ID 21; Konstantin Ignatyev, the I18 beamline staff, and the Diamond Light Source Synchrotron for their support through the experiment SP23348-1; Manfred Burghammer, European Synchrotron Radiation Facility, for giving additional "in-house" beamtime at ID 13 (data not shown); Tom Vosch, Department of Chemistry, University of Copenhagen, for attempting to obtain new Raman and UV-Vis spectra of samples 5 and 10 (data not shown); and Irina Snigireva, European Synchrotron Radiation Facility, for scanning electron microscopy-energy dispersive X-ray spectroscopy analysis of organic binders (data not shown).

1. T. Christiansen, Manufacture of black ink in the ancient Mediterranean. *Bull. Am. Soc. Papyrol.* **54**, 167–195 (2017).
2. I. Rabin, O. Hahn, T. Wolff, T. A. Masic, G. Weinberg, On the origin of the ink of the Thanksgiving Scroll (1QHodayot[a]). *Dead Sea Discov.* **16**, 97–106 (2009).
3. A. Lucas, *Ancient Egyptian Materials and Industries*, revised and enlarged by J. R. Harris, (Edward Arnold, ed. 4, 1962).
4. C. Gallazzi, G. Hadji-Minaglou, Eds. *N. Litinas, Scribe's palet in Trésors inattendus: 30 ans de fouilles et de coopération à Tebtynis (Fayoum)* (Institut Francais d'Archéologie Orientale, 2019).
5. M. S. Pinarello, *An Archaeological Discussion of Writing Practice: Deconstruction of the Ancient Egyptian Scribe* (Golden House Publications, 2015).
6. C. Brøns, M.-L. Sargent, "Pigments and Dyes: The use of madder lake for the depiction of garments on ancient Egyptian mummy portraits in the Ny Carlsberg Glyptotek in Textiles and dyes in the Mediterranean economy and society" in *Proceedings Sixth International Symposium in Ancient Mediterranean World* (Padova–Este–Altino, Italy), M. S. Busana, M. Gleba, F. Meo, A. R. Tricomi, Eds. (Libros Portico, 2018), pp. 481–490.

7. T. Ghigo, I. Rabin, P. Buzi, Black Egyptian inks in Late Antiquity: New insights on their manufacture and use. *Archaeol. Anthropol. Sci.* **12**, 1–14 (2020).
8. C. Chiappe, C. S. Pomelli, S. Sartini, Combined use of scanning electron microscopy – energy-dispersive X-ray spectroscopy and Fourier transform infrared imaging coupled with principal component analysis in the study of ancient Egyptian papyri. *ACS Omega* **4**, 22041–22047 (2019).
9. T. Arlt *et al*., Absorption edge sensitive radiography and tomography of Egyptian papyri. *J. Cult. Herit.* **39**, 13–20 (2019).
10. I. Rabin, M. Krutzsch, "The writing surface of papyrus and its materials. 1. Can the writing material papyrus tell us where it was produced? 2. Material studies of the inks" in *Proceedings of the 28th Congress of Papyrology Barcelona 1–6 August 2016*, A. Nodar, S. T. Tovar, Eds. (Montserrat, 2019), pp. 773–781.
11. G. Festa *et al*., Egyptian metallic inks on textiles from the 15th century BCE unravelled by non-invasive techniques and chemometric analysis. *Sci. Rep.* **9**, 7310 (2019).
12. C. Collini *et al*., The quest for mixed inks. *Manuscript Cultures* **11**, 41–46 (2018).
13. T. Christiansen *et al*., The nature of ancient Egyptian copper-containing carbon inks is revealed by synchrotron radiation based X-ray microscopy. *Sci. Rep.* **7**, 15346 (2017).
14. T. Christiansen *et al*., Chemical characterization of black and red inks inscribed on ancient Egyptian papyri: The Tebtunis temple library. *J. Archaeol. Sci. Rep.* **14**, 208–219 (2017).
15. E. Brun *et al*., Revealing metallic ink in Herculaneum papyri. *Proc. Natl. Acad. Sci. U.S.A.* **113**, 3751–3754 (2016).
16. P. Tack *et al*., Tracking ink composition on Herculaneum papyrus scrolls: Identification, localization, quantification and speciation of lead by X-ray based techniques and Monte Carlo simulations. *Sci. Rep.* **6**, 20786 (2016).
17. S. Cersoy *et al*., Identifying and quantifying amorphous and crystalline content in complex powdered samples: Application to archaeological carbon blacks. *J. Appl. Cryst.* **49**, 585–593 (2016).
18. C. Canevali *et al*., A multi-analytical approach for the characterization of powders from the Pompeii archaeological site. *Anal. Bioanal. Chem.* **401**, 1801–1814 (2011).
19. B. Wagner *et al*., Analytical approach to the conservation of the ancient Egyptian manuscript "Bakai Book of the Dead": A case study. *Mikrochim. Acta* **159**, 101–108 (2007).
20. É. Delange, M. Grange, B. Kusko, E. Menei, Apparition de l'encre Métallogallique en Égypte à partir de la Collection de Papyrus du Louvre. *Rev. Egyptol.* **41**, 213–217 (1990).
21. D. A. Scott, A review of ancient Egyptian pigments and cosmetics. *Stud. Conserv.* **61**, 185–202 (2014).
22. L. M. di Stefano, R. Fuchs, Characterisation of the pigments in a Ptolemaic Egyptian Book of the Dead Papyrus. *Archaeol. Anthropol. Sci.* **3**, 229–334 (2011).
23. L. Lee, S. Quirke, "Painting materials" in *Ancient Egyptian Materials and Technology*, P. T. Nicholson, I. Shaw, Eds. (Cambridge University Press, 2000), pp. 104–120.
24. K. Ryholt, "Libraries from the Late Period and Graeco-Roman Egypt. c. 800 BCE–200 CE" in *Libraries Before Alexandria. Near Eastern Traditions*, K. Ryholt, G. Barjamovic, Eds. (Oxford University Press, 2019), pp. 390–470.
25. C. Gallazzi, "Appendice" in *Tebtynis VI: Scripta Varia*, C. Gallazzi, Ed. (Institut Français d'Archéologie Orientale, 2018), pp. 113–172.
26. K. Ryholt, "On the contents and nature of the Tebtunis temple library. A status report" in *Tebtynis und Soknopaiu Nesos. Leben im Römerzeitlichen Fajum. Akten des Internationalen Symposions vom 11. bis 13. Dezember in Sommerhausen bei Würzburg*, S. Lippert, M. Schentuleit, Eds. (Harrassowitz Verlag, 2005), pp. 141–170.
27. F. Hagen, K. Ryholt, *The Antiquities Trade in Egypt 1880–1930: The H. O. Lange Papers* (Det Kongelige Danske Videnskabernes Selskab, 2016), pp. 178–179.
28. Pliny, *Natural History in Ten Volumes with an English Translation by H. Rackham* (Heinemann Ltd., 1938), Book XXXV.
29. J. K. Delaney, K. A. Dooley, R. Radpour, I. Kakoulli, Macroscale multimodal imaging reveals ancient painting production technology and the vogue in Greco-Roman Egypt. *Sci. Rep.* **7**, 15509 (2017).
30. M. S. Walton, K. Trentelman, Romano-Egyptian red lead pigment: A subsidiary commodity of Spanish silver mining and refinement. *Archaeometry* **51**, 845–860 (2009).
31. I. Kakoulli, Late Classical and Hellenistic painting techniques and materials: A review of the technical literature. *Rev. Conserv.* **3**, 56–67 (2002).
32. G. Casalino, N. del Buono, C. Mencar, "Nonnegative matrix factorizations for intelligent data analysis" in *Non-negative Matrix Factorization Techniques: Advances in Theory and Applications*, G. R. Naik, Ed. (Springer, 2016), pp. 49–74.
33. S. Sra, I. S. Dhilon, "Generalized nonnegative matrix approximations with Bregman divergences" in *Advances in Neural Information Processing Systems*, Y. Weiss, B., Scholkopf, J. C. Platt Eds. (NIPS, 2005), vol. 18, pp. 1–8.
34. A. K. Singh, B. K. Jain, K. Chandra, Mössbauer studies of naturally occurring red ochre and yellow ochre. *J. Appl. Phys. D: Appl. Phys.* **11**, 55–62 (1978).
35. H. Bearat, "Les pigments à base de plomb en peinture murale Romaine" in Conservation et restauration des biens culturels: Pierre, pollution, atmosphérique, peinture murale, études scientifiques et cas pratiques, R. Pancella, Ed. (École Polytechnique Fédérale de Lausanne, 1996), pp. 547–555.
36. P. Holakooei, J. F. de Lapérouse, M. Rugiadi, F. Carò, Early Islamic pigments at Nishapur, north-eastern Iran: Studies on the painted fragments preserved at the Metropolitan Museum of art. *Archaeol. Anthropol. Sci.* **10**, 175–195 (2018).
37. C. Remazeilles, E. Conforto, A buried Roman bonze inkwell: Chemical interactions with archaeological fertilizers. *Stud. Conserv.* **53**, 110–117 (2008).
38. S. Sotiropoulo *et al*., Lead pigments and related tools at Akrotiri, Thera, Greece. Provenance and application techniques. *J. Archaeol. Sci.* **37**, 1830–1840 (2010).
39. E. Welcomme, "Development de techniques combines de microanalyse par rayonnement de synchrotron pour l'etude des pigments a base des pigments a base carbonates de plomb," PhD thesis, University of Pierre and Marie Curie, Paris, France (2017).
40. J. Twilley, K. M. Garland, "Materials and deterioration phenomena in a Yuan Dynasty wall painting in Scientific research on the pictorial arts of Asia" in *Proceedings of the 2nd Forbes Symposium at the Freer Gallery of Art*, P. Jett, J. Winter, B. McCarthy, Eds. (Archetype Publications, 2005), pp. 109–119.
41. V. Laperche, S. J. Traina, P. Gaddam, T. J. Logan, Chemical and mineralogical characterizations of contaminated soil: Reactions with synthetic apatite. *Environ. Sci. Technol.* **30**, 3321–3326 (1996).
42. N. Salvadó *et al*., Identification of reaction compounds in micrometric layers from Gothic paintings using combined SR-XRD and SR-FTIR. *Talanta* **79**, 419–428 (2009).
43. A. van Loon *et al*., Beauty is skin deep: The skin tones of Vermeer's *Girl with a Pearl Earring*. *Herit. Sci.* **7**, 102 (2019).
44. S. De Meyer *et al*., Imaging secondary reaction products at the surface of Vermeer's *Girl with the Pearl Earring* by means of macroscopic X-ray powder diffraction scanning. *Herit. Sci.* **7**, 67 (2019).
45. S. W. T. Price *et al*., Unravelling the spatial dependency of the complex solid-state chemistry of Pb in a paint micro-sample from Rembrandt's *Homer* using XRD-CT. *Chem. Commun. (Camb.)* **55**, 1931–1934 (2019).
46. A. van Loon *et al*., Artificial orpiment, a new pigment in Rembrandt's palette. *Herit. Sci.* **5**, 26 (2017).
47. S. Aze, J. M. Vallet, A. Baronnet, O. Grauby, The fading of red lead pigment in wall paintings: Tracking the physico-chemical transformations by means of complementary micro-analysis techniques. *Eur. J. Mineral.* **18**, 835–843 (2006).
48. P. Martinetto *et al*., Synchrotron X-ray micro-beam studies of ancient Egyptian make-up. *Nucl. Instrum. Methods Phys. Res. B* **181**, 744–748 (2001).
49. J. Salvant *et al*., A Roman Egyptian painting workshop: Technical investigation of the portraits from Tebtunis, Egypt. *Archaeometry* **60**, 815–833 (2017).
50. A. Monson, "Salinization and agricultural productivity" in *The Fayyum in Das Fayyûm in Hellenismus und Kaiserzeit: Fallstudien zu multikulturellem Leben in der Antike*, C. Arlt, M. A. Stadler, Eds. (Harassowitz Verlag, 2013), pp. 123–140.
51. A. Lucas, *A Preliminary Investigation of the Soil and Water of the Fayum Province* (Public Works Ministry, Survey Department, 1902).
52. A. Accardo *et al*., Amyloid β peptide conformational changes in the presence of a lipid membrane system. *Langmuir* **30**, 3191–3198 (2014).
53. A. H. Sabin, *Industrial and Artistic Technology of Paint and Varnish* (J. Wiley & Sons, 1927).
54. M. L. Karstens, F. R. Hansen, Drier soap manufacture. *Ind. Eng. Chem.* **41**, 2080–2090 (1949).
55. R. Halleux, *Les Alchimistes Grecs, Tome 1: Papyrus de Leyde, Papyrus de Stockholm. Fragments de Recettes* (Les Belles Letres, 1981).
56. E. R. Cale, The Stockholm papyrus. An English translation with brief notes. *J. Chem. Educ.* **4**, 979–1002 (1926).
57. K. Dosoo, A history of the Theban magical library. *Bull. Am. Soc. Papyrol.* **53**, 251–274 (2016).
58. J. Maroger, *The Secret Formulas and Techniques of the Masters* (translated from French by E. Beckham) (Studio Publications, 1948).
59. M. Cotte *et al*., Lead soaps in paintings: Friends or foes? *Stud. Conserv.* **62**, 2–23 (2017).
60. M. Cotte, P. Dumas, G. Richard, R. Breniaux, P. Walter, New insight on ancient cosmetic preparation by synchrotron-based infrared microscopy. *Anal. Chim. Acta* **553**, 105–110 (2005).
61. W. Wrezinski, *Der Papyrus Ebers* (J. C. Hinrichs'sche Buchhandlung, 1903), (translation from ancient Egyptian by T. Christiansen).
62. P. Martinetto, M. Anne, E. Dooryhée, G. Tsoucaris, P. Walter, "A synchrotron X-ray diffraction study of Egyptian cosmetics" in *Radiation in Art and Archaeometry*, D. C. Creagh, D. A. Bradly, Eds. (Elsevier, 2000), pp. 297–316.
63. J. R. Harris, *Lexicographical Studies in Ancient Egyptian Minerals* (Akademie Verlag, 1961).
64. R. Fuchs, L. M. di Stefano, "Untersuchungen einer altägyptischen Malerei der 18. Dynastie" in *Die Erfindung der körperlicher Darstellung in der altägyptischer Kunst in Metalla Sonderheft 3*, A. Hauptmann, O. Hahn, Eds. (Deutsches Bergbaumuseum, 2010), pp. 158–160.
65. M. Cotte *et al*., Blackening of Pompeian cinnabar paintings: X-Ray microspectroscopy analysis. *Anal. Chem.* **78**, 7484–7492 (2006).
66. F. Cariati, L. Rampazzi, L. Toniolo, A. Pozzi, Calcium oxalate films on stone surfaces: Experimental assessment of the chemical formation. *Stud. Conserv.* **45**, 180–188 (2000).
67. M. Cotte, P. Walter, G. Tsoucaris, P. Dumas, Studying skin of an Egyptian mummy by infrared microscopy. *Vib. Spectrosc.* **38**, 159–167 (2005).
68. E. Grill, S. Löffler, E. L. Winnacker, M. H. Zenk, Phytochelatins, the heavy-metal-binding peptides of plants, are synthesized from glutathione by a specific γ-glutamylcysteine dipeptidyl transpeptidase (phytochelatin synthase). *Proc. Natl. Acad. Sci. U.S.A.* **86**, 6838–6842 (1989).
69. F. el-Baz, *The Geology of Egypt: An Annotated Bibliography* (E. J. Brill, 1984).
70. K. Dahm, The stylus revealed: A metalpoint identification study of fifteenth-and sixteenth-century Italian drawings in the Metropolitan Museum of Art. *Pap. Conserv.* **28**, 75–86 (2004).
71. M. Cotte *et al*., Kinetics of oil saponification by lead salts in ancient preparations of pharmaceutical lead plasters and painting lead mediums. *Talanta* **70**, 1136–1142 (2006).
72. T. S. Wong, T.-H. Chen, X. Shen, C.-M. Ho, Nanochromatography driven by the coffee ring effect. *Anal. Chem.* **83**, 1871–1873 (2011).